# Flexural behavior and analysis of prestressed ultra-high-performance concrete beams made from locally available materials

Andrew J. Giesler, Michael J. McGinnis, and Brad D. Weldon

- This research focused on the design, flexural testing, and analysis of three large-scale prestressed beams using ultra-high-performance concrete made from materials local to the state of New Mexico.
- Parameters varied among the prestressed specimens and included the removal of all mild steel reinforcement and the effect of a composite cast-in-place concrete deck.
- Experimental strengths were compared to design strengths according to the American Association of State Highway and Transportation Officials' *AASHTO LRFD Bridge Design Specifications*.

Throughout the past few decades, significant effort has been given to the development of ultra-high-performance concrete (UHPC) and its introduction into structural design. A large portion of this effort has been directed toward its use in precast, prestressed concrete applications, particularly for bridges. The U.S. Federal Highway Administration launched a project in 2001 that focused on familiarizing the concrete and transportation industries with UHPC and emphasized its performance in precast, prestressed concrete bridge superstructures.[1] This project demonstrated many of the benefits of UHPC, but a variety of questions pertinent to the development of standardized procedures for design and production remain unanswered. Currently, there are no U.S. design codes for the use of UHPC.

UHPC has the potential to improve U.S. transportation infrastructure. Its benefits over conventional concrete include slimmer members, longer spans, reduced material quantities, reduced steel detailing and reinforcement, decreased construction time, decreased maintenance, increased durability, and an increased design life. The use of nonproprietary UHPCs can help to increase the economical value of this product; however, for structural design, it is necessary to ensure that mechanical properties are consistent and reliable.

Over the past several years, a research program investigated the potential of implementing UHPC developed with materials local to New Mexico into bridge design. Weldon et al.[2] and Taylor et al.[3] evaluated the feasibility of UHPC that used readily available New Mexico aggregates for its effective-

ness in bridge superstructure design. By introducing local materials into the mixture proportions, it was shown that there was an overall life-cycle savings associated with using locally developed UHPC compared with conventional concrete. Mixture proportions (Weldon et al.[4]) were developed to achieve quality mechanical and durability properties while creating a more economical UHPC by increasing the size and content of aggregates, supplementing silica fume with Class F fly ash, and developing an efficient and economical curing regimen.[5]

The durability of the UHPC mixture proportions using local materials was evaluated by investigating resistance to freezing and thawing, alkali-silica reaction, and delayed ettringite formation that might be caused by the high curing temperatures. The results from these investigations showed that the mixture proportions provide superior performance and are similar to results from other studies that have demonstrated UHPC to be exceptionally durable.[4,6–8] Furthermore, Giesler et al.[9] worked with precasters to implement the locally developed UHPC. Through the process, the UHPC was successfully cast and cured with no changes to the precast concrete facility's equipment.

To investigate the flexural behavior of the locally developed UHPC, a normally reinforced two-span bridge located in southern New Mexico was redesigned with prestressed girders using the locally developed UHPC. Three scaled prestressed UHPC beam specimens were adapted from the full-scale girder design and were cast and cured at a local precast concrete facility. The beams were then tested to evaluate the flexural capacity of the prestressed specimens. The results provide a foundation for the implementation of nonproprietary UHPC in bridge applications in New Mexico and, potentially, regional infrastructure.

## Material properties

### Concrete

The nonproprietary UHPC mixture proportions were developed from regionally available materials, with the exception of the steel fibers, which came from a national distributor. The UHPC had a water–cementitious material ratio (*w/cm*) of 0.145 and a design compressive strength of 22,000 psi (150 MPa). **Table 1** provides the UHPC mixture proportions assuming aggregates at oven-dry conditions and a 1.5% fiber content by volume. The fiber content was selected based on previous studies to balance material properties and economy.[4,5] The fiber used was a monofilament fiber with a diameter of 0.008 in. (0.2 mm) and a length of 0.50 in. (13 mm). According to the material data sheet, the minimum tensile strength of the fibers was 285 ksi (1970 MPa) with a modulus of elasticity of 29,000 ksi (200 GPa). Fine angular sand with a maximum particle size of 0.19 in. (4.8 mm) and minimum particle size of 0.003 in. (0.08 mm) was used. The high-range water-reducing admixture used was polycarboxylate based with a unit weight of 71.76 lb/ft$^3$ (1149 kg/m$^3$). Details on the mixing procedure can be found in Giesler et al.[9]

**Table 1.** Ultra-high-performance concrete mixture proportions using local materials (1.0 yd$^3$ batch)

| Constituent | Quantity, lb |
|---|---|
| Angular sand | 1812 |
| Type I/II cement | 1296 |
| Silica fume | 203 |
| Class F fly ash | 122 |
| Water | 258 |
| High-range water-reducing admixture | 82.1 |
| Steel fibers | 198 |

Note: 1 yd$^3$ = 0765 m$^3$. 1 lb = 0.455 kg.

Guaderrama and Weldon[10] experimentally found the average modulus of elasticity $E_c$ for the UHPC to be 6065 ksi (41.82 GPa). The experimental results were compared to several prediction equations, and the best-fit equation to estimate $E_c$ was determined to be Eq. (1) developed by Graybeal.[8]

$$E_c = 46.2\sqrt{f_c'} \quad (1)$$

where

$f_c'$ = concrete compressive strength, psi

For units in MPa, the constant in Eq. (1) is 3836.

Following ASTM C78,[11] Visage[12] found that the average modulus of rupture $f_r$ (that is, first cracking) of the UHPC with the steel fibers was approximately 1.33 ksi (9.17 MPa), regardless of the fiber content. First cracking was identified through the use of displacement transducers placed on the side face of the modulus-of-rupture specimens during testing. The prediction equations provided in the American Association of State Highway and Transportation Officials' *AASHTO LRFD Bridge Design Specifications*[13] and in Graybeal[8] are similar, and both underestimate the modulus of rupture observed by Visage. The slightly more conservative estimation provided in the AASHTO LRFD specifications was used for design.

UHPC possesses significant postcracking tensile capacity due to the pull-out strength of crack-bridging steel fibers, which should be considered in design. **Figure 1** (dashed curve) shows the fiber behavior as observed in direct tension tests on UHPC dog-bone specimens performed by Naaman and Reinhardt.[14] This behavior is modeled as a multilinear stress distribution in several design guidelines.[15–17]

To simplify the estimation process, the contribution of the fibers on the strength of the girder was determined using an equivalent uniform tensile stress block that acted from

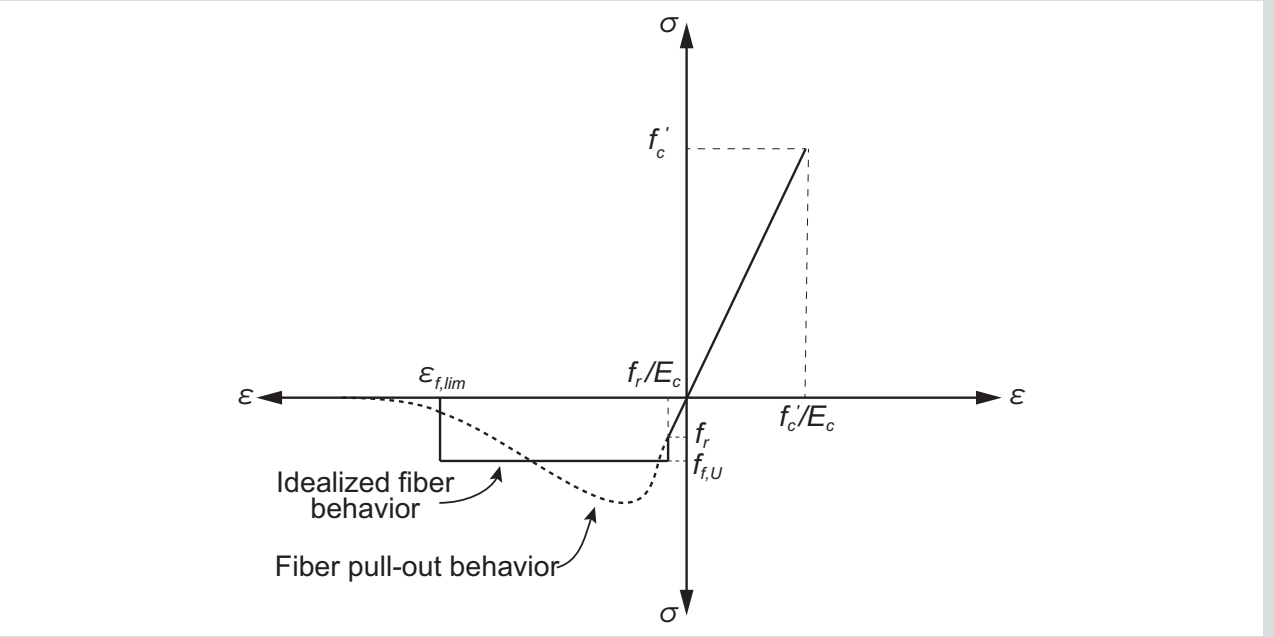


**Figure 1.** Analytical stress-strain relationship for ultra-high-performance concrete (not to scale). Note: $E_c$ = concrete modulus of elasticity; $f'_c$ = specified compressive strength of concrete; $f_{f,U}$ = tensile strength of crack-bridging fibers; $f_r$ = modulus of rupture; $\varepsilon$ = strain; $\varepsilon_{f,lim}$ = ultimate tensile strain; $\sigma$ = stress.

the depth of the primary reinforcement to the neutral axis depth developed by Visage[12] for the locally developed UHPC and is similar to a procedure presented by Graybeal.[8] The tensile strength of the crack-bridging fibers $f_{f,U}$ is equal to the fiber content (% by volume) $v_f$ multiplied by a fiber stress distribution factor $\beta_f$, which is used to approximate the fiber stress distribution as an equivalent rectangular stress block (Eq. [2]).

$$f_{f,U} = \beta_f v_f \quad (2)$$

The factor $\beta_f$ was determined experimentally from modulus-of-rupture tests and for the fibers used was determined to be 0.25 ksi (1.72 MPa).[12] The value for the ultimate tensile strain $\varepsilon_{f,lim}$ at complete fiber pullout was assumed to be 0.01. The compressive strength was assumed to act linearly to $f'_c$, which is the typical observed behavior during compression tests.[10,16,18] The solid line in Fig. 1 shows the assumed compressive and tensile stress-strain behavior of the UHPC.

One of the three beams tested had a cast-in-place high-strength concrete (HSC) composite deck with a 28-day design compressive strength of 8.0 ksi (55 MPa). For the HSC, 4.0 and 6.0 in. (100 and 150 mm) cylinders were used for compressive strength measurements following ASTM C39.[19] For the UHPC, 2.0 and 4.0 in. (50 and 100 mm) cubes were cast to eliminate the need for difficult end preparation on cylindrical specimens. British Standard 1881[20] was used for the testing of the cube specimens. **Table 2** gives the average measured compressive strength results as well as additional information, including the *w/cm* ratio, fiber content $v_f$, specimen geometry, compressive strength of the concrete at

**Table 2.** Concrete compressive strength summary

| Concrete | *w/cm* | $v_f$, % | Design strength, ksi | Specimen geometry, in. | $f_{c,7day}$, ksi | $f_{c,28day}$, ksi | $f_{c,test}$, ksi |
|---|---|---|---|---|---|---|---|
| Ultra-high-performance concrete | 0.145 | 1.5 | 22.0 | 2.0 cube | 24.4 | n/a | 22.0 |
| | | | | 4.0 cube | 23.9 | n/a | 22.6 |
| High-performance concrete | 0.226 | 0 | 8.0 | 6.0 × 12 cylinder | n/a | 8.77 | 8.21 |
| | | | | 4.0 × 8.0 cylinder | n/a | n/a | 9.50 |

Note: $f_{c,7day}$ = concrete compressive strength at seven days; $f_{c,28day}$ = concrete compressive strength at 28 days; $f_{c,test}$ = test day compressive strength; n/a = not applicable because no specimens were tested; $v_f$ = fiber content as percentage of volume; *w/cm* = water–cementitious material ratio. 1 in. = 25.4 mm; 1 ksi = 6.895 MPa.

seven days $f_{c,7day}$ for UHPC batches or 28 days $f_{c,28day}$ for HSC batches, and test-day compressive strength $f_{c,test}$.

## Mild steel reinforcement

Two beam specimens contained no. 3 (10M) mild steel reinforcement used as shear reinforcement in the form of stirrups. The design yield for the reinforcement was 60 ksi (410 MPa); however, to obtain a more accurate value, four samples of the no. 3 reinforcing bar were tested in tension. The average yield stress was 63.7 ksi (439 MPa), the average modulus of elasticity was 26,600 ksi (183 GPa), and the average maximum stress was 97.6 ksi (673 MPa).

## Prestressing strand

The prestressing strand was 0.6 in. (15 mm) diameter, Grade 270 (1860 MPa) low-relaxation strands. The yield strength $f_{py}$ was assumed according to the AASHTO LRFD specifications[13] to be 90% of the ultimate strand tensile strength $f_{pu}$ ($f_{py}$ equal to $0.90f_{pu}$). The modulus of elasticity of the strand was provided in the supplier specifications as 28,800 ksi (199 GPa).

## Design of girder specimens

A structurally deficient bridge was selected for replacement using UHPC girders. The bridge is composed of two simply supported spans with lengths of 25 ft (7.6 m). The nine girders that make up each span are 36 in. (910 mm) wide, mild steel-reinforced precast concrete channel beams. The bridge supports two design lanes, has a transverse width from curb to curb of approximately 25 ft, and a total width from out to out of 27 ft (8.2 m).

The 2012 AASHTO LRFD specifications,[13] with modifications for UHPC properties, was followed for the design of the UHPC girders. Modifications were made to account for the postcracking tensile strength contributed by the fibers and for the compressive stress distribution characteristic of UHPC. The chosen girder shape was reflective of the current channel shape to take advantage of the substructure configuration and eliminate the need for a composite deck. The span length was maintained at 25.0 ft (7.62 m); however, the girder width was increased from 36 to 48 in. (910 to 1220 mm).

**Figure 2** shows the preliminary dimensions of a full-scale UHPC replacement girder. Full details of the design of the preliminary bridge girders can be found in Giesler.[21] The goal was not to test a section that was optimized using the advanced properties of UHPC, but rather to provide an understanding of the flexural behavior of the preliminary design for the bridge replacement.

The moment capacity of the section $\phi M_n$ (where $\phi$ is the strength-reduction factor and $M_n$ is the nominal moment strength), including the contribution of the fibers, was determined using Eq. (3). The value of $\phi$ corresponds to the LRFD strength-reduction factor for flexure, taken as 1.0 for prestressed concrete.

$$\phi M_n = \phi[(A_{ps}f_{ps}z_{ps}) + (A_s f_s z_s) + (A_f f_{f,U} z_f)] \quad (3)$$

where

$A_{ps}$ = prestressing strand area

$f_{ps}$ = stress at the centroid of prestressing strands at ultimate loads

$z_{ps}$ = distance between the resultants of the tension in the prestressing strands and the compression in the concrete

$A_s$ = longitudinal mild steel reinforcement area

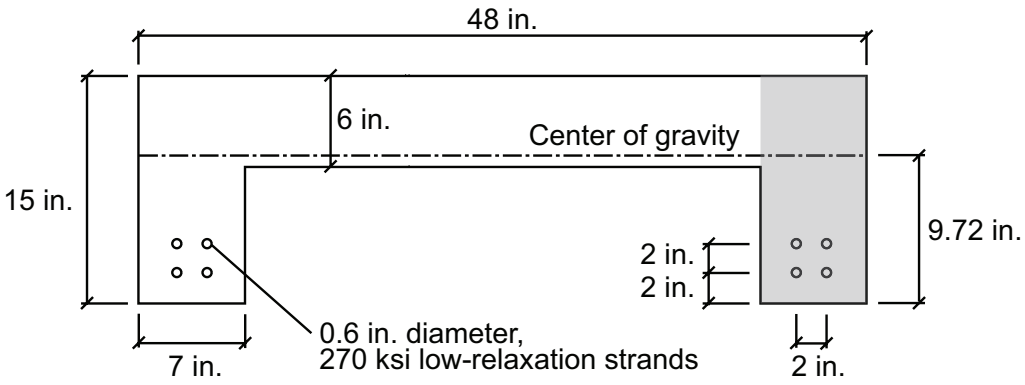


**Figure 2.** Preliminary full-scale ultra-high-performance concrete replacement prestressed girder. Note: 1 in. = 25.4 mm; 1 ksi = 6.895 MPa.

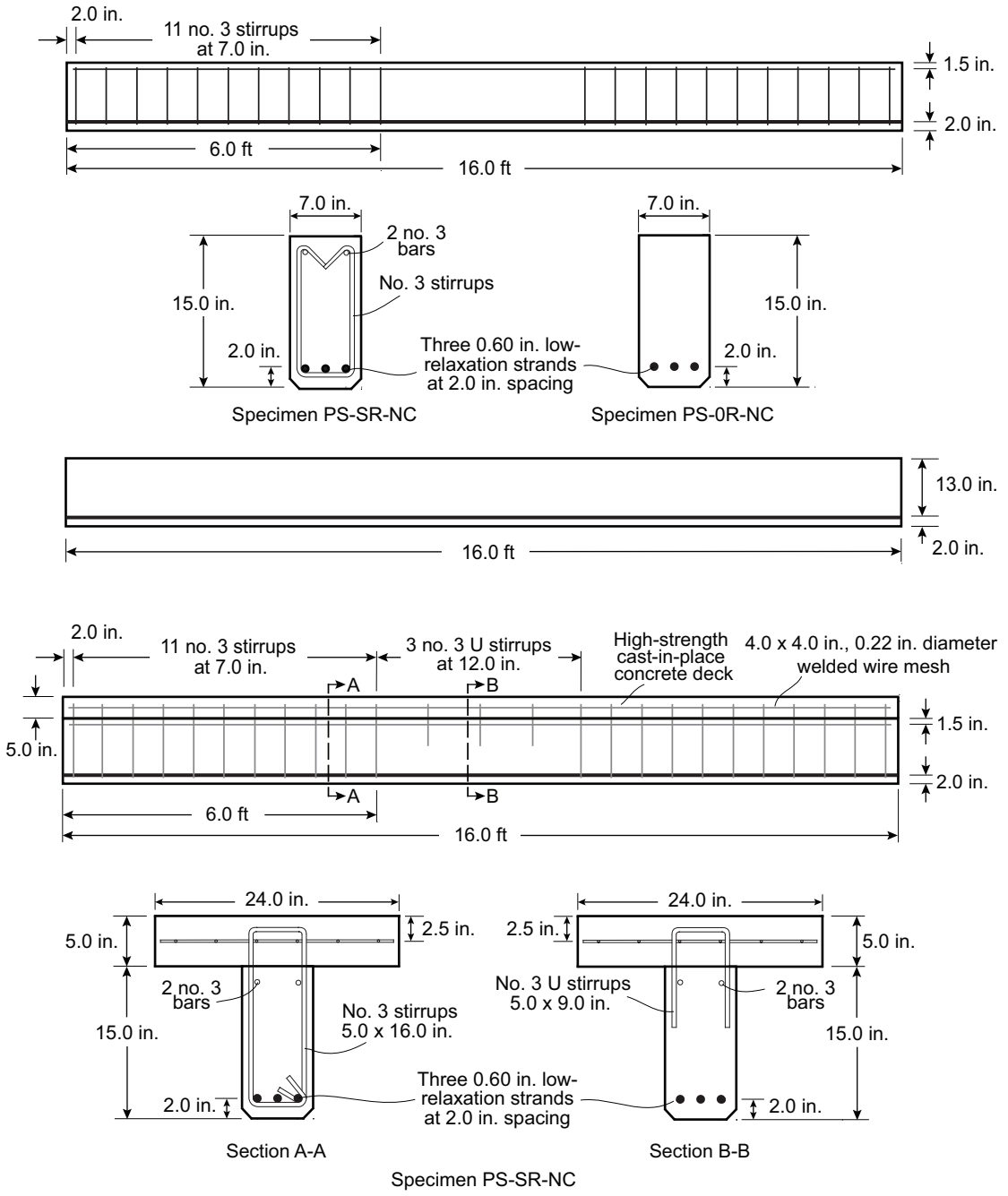


**Figure 3.** Prestressed concrete beam details. Note: no. 3 = 10M; 1 in. = 25.4 mm; 1 ft = 0.305 m.

$f_s$ = stress in the mild steel reinforcement

$z_s$ = distance between the resultants of the force in the mild steel and the compression in the concrete

$A_f$ = area of the cross section in tension between the neutral axis and centroid of prestressing steel

$z_f$ = distance between the resultant of the fiber tensile strength and the concrete compression resultant

The presence of steel fibers in UHPC can provide significant shear capacity. By incorporating the fiber contribution into design equations, the need for mild steel reinforcement can be partially or completely eliminated. The AASHTO LRFD spec-

ifications[13] currently have no specifications for evaluating the shear strength contribution of the fibers in UHPC. The equations used in this study are from the recommendations for the design of UHPC by Ulm[22] and AFGC/SETRA.[15] The factored shear strength, including the fiber contribution, of the section $\phi_v V_n$ (where $\phi_v$ is the strength-reduction factor for shear and $V_n$ is the nominal shear strength) is calculated using Eq. (4).

$$\phi_v V_n = \phi_c V_c + \phi_s V_s + V_p + \phi_f V_f \quad (4)$$

$\phi_c$ = strength-reduction factor of concrete based on the material variability = 0.66

where

$V_c$ = shear strength of concrete

$\phi_s$ = LRFD mild steel strength-reduction factor for shear = 0.9

$V_s$ = shear strength of the mild steel shear reinforcement

$V_P$ = shear strength of prestressing strand

$\phi_f$ = strength-reduction factor of steel fibers to account for the variability of fiber dispersion = 0.66

$V_f$ = shear strength from the steel fibers

The preliminary girder (Fig. 2) was found to have excess capacity for both shear and moment, resulting in the design being controlled by service conditions. The girder geometry and strand configuration are a preliminary design and would need modifications before final girder fabrication.

## Scaled beam adaptation

For testing, three scaled 16 ft (4.9 m) long UHPC specimens were designed to reflect the geometry of one stem of the UHPC channel girder (shaded in gray in Fig. 2). The beams had a width of 7 in. (180 mm) and a height of 15 in. (380 mm). The specimens were designed with one layer of prestressing strands consisting of three 0.6 in. (15 mm) diameter low-relaxation strands placed 2.0 in. (50 mm) from the bottom face of the beam. The initial prestressing force $P_i$ after transfer was 90.0 kip (400 kN). **Figure 3** shows the three beam cross sections and profiles.

Specimen PS-SR-NC was designed assuming no fiber contribution to shear resistance. The design procedure followed the recommendations in the AASHTO LRFD specifications[13] and resulted in 11 no. 3 (10M) stirrups at 7.0 in. (180 mm) spacing beginning 2.0 in. (51 mm) from each end face of the specimen. Near midspan of the beam, no shear reinforcement was included to limit its effect on the flexural behavior.

The effect of eliminating all transverse mild steel shear reinforcement was investigated through the testing of specimen PS-0R-NC. UHPC has significantly increased shear capacity due to the addition of steel fibers; thus, the concrete and fibers provided the required shear capacity. The design and casting of this beam was simplified due to the elimination of the mild steel reinforcement, one of the benefits attributed to the contribution of steel fibers. The only reinforcement in the beam consisted of the three prestressing strands. No observable cracking or other problems were observed at prestress transfer.

Specimen PS-SR-C was similar to the design of specimen PS-SR-NC; however, a cast-in-place composite HSC deck

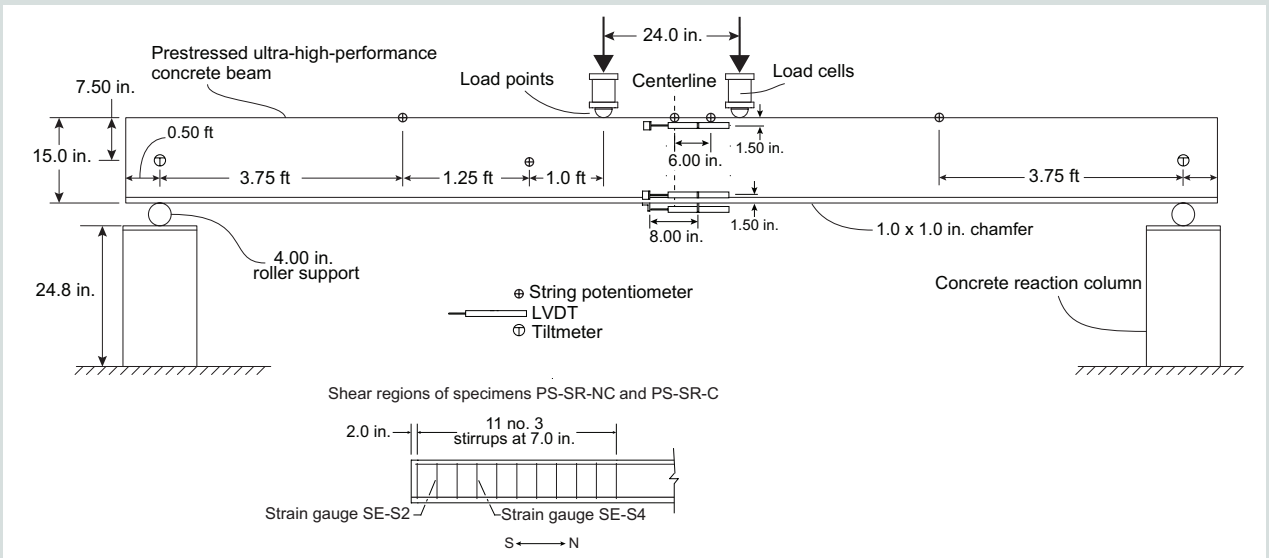


**Figure 4.** Test setup and instrumentation. Note: LVDT = linear variable displacement transducer; UHPC = ultra-high-performance concrete. No. 3 = 10M; 1 in. = 25.4 mm; 1 ft = 0.305 m.

was placed before testing. The interface shear resistance at the deck and beam slip plane was determined according to the AASHTO LRFD specifications,[13] assuming the top surface of the beam was smooth. The mild steel shear reinforcement extended past the top surface of the girder to provide interface shear reinforcement for the placement of the deck. In addition, three mild steel bars bent into U shapes were placed throughout the midspan to prevent separation of the deck and beam. Due to the loading configuration, full hoops were eliminated from this region to minimize its effect on the flexural behavior of the section. A 2 ft (0.6 m) wide, 5.0 in. (130 mm) thick deck reinforced with a 4.0 × 4.0 in. (100 × 100 mm) welded-wire mesh with a wire diameter of 0.22 in. (5.7 mm) placed at middepth was cast on the beam.

## Instrumentation and test setup

**Figure 4** shows the test setup and instrumentation. The load was applied to the specimen at two points spaced 2.0 ft (0.61 m) apart centered at midspan, creating a nearly constant moment region. The span length between roller supports was 15.0 ft (4.57 m) for all specimens. To prevent crushing of the concrete at the rollers, steel plates were cast into the beams at the beam ends and also helped to minimize axial effects developed due to constraint at the reactions. The beams were loaded in flexure using a displacement rate of approximately 0.01 in./min (0.25 mm/min).

Embedded vibrating-wire strain gauges were used to record internal strains in the concrete at the level of the prestressing strands. Using the embedded vibrating-wire strain gauges, the initial and effective prestressing forces were determined. Although it was not possible to determine the individual source of the losses using this type of sensor, the overall losses were determined, providing an accurate estimate of the effective prestressing force at the time of testing. Each gauge was placed approximately 1.0 ft (0.30 mm) from midspan in an effort to reduce the potential for the gauge to influence failure in the flexural region.

The total load applied to the specimens was measured using two load cells placed at the points of load application. The total force applied to the specimen was the sum of the load cell forces.

Due to the strength of the steel fibers and their ability to prevent diagonal shear cracks from propagating, little contribution from the mild steel shear reinforcement (when present) was expected. However, to evaluate whether the fibers were able to carry the shear forces that developed in the shear region, surface-bonded strain gauges were placed on two stirrup legs close to the support on the southeast end of the beam (Fig. 4).

Two linear variable displacement transducers were placed on the west vertical face of the specimens at 1.50 in. (38.1 mm) from the top and bottom faces of the specimens. An additional linear variable displacement transducer was placed at the center of the bottom face to measure the extreme tensile strain of the specimen. An 8 in. (200 mm) gauge length between the anchor points of the linear variable displacement transducers and the reaction plates was created at the beam midspan, and the measurements were used to determine the curvature of the beam.

Specimen deflections were captured with linear string potentiometers. Two string potentiometers were connected near midspan and one slightly offset from midspan (in case one was lost due to cracking), one directly at midspan and one at both quarter points of the span. For the testing of specimen PS-SR-C, an additional string potentiometer attached to the top surface of the composite HSC deck was placed directly at the beam centerline. This was used to monitor any separation between the prestressed UHPC beam and the cast-in-place deck, indicating noncomposite behavior.

## Prestressing forces

The specimens were cured under steam treatment for approximately four days, followed by one and a half additional days of dry heat. The full-curing regimen was completed before the release of prestressing forces into the specimens to ensure that the desired strengths were met.

**Table 3** gives the initial and effective prestressing forces measured by the embedded vibrating-wire strain gauges. Larger prestressing forces were measured for specimen PS-SR-NC. This specimen was cast in a separate bed where the strands had a higher initial stress. The other two specimens were cast in line and showed similar initial prestressing forces. The tensile stresses at the tops of the beams at release were designed to be close to the modulus of rupture of the UHPC; however, no signs of cracking or significant camber were observed. The effective prestressing forces were measured at the time of testing.

## Flexural behavior, results, and comparison

**Figure 5** plots the load versus deflection and moment versus curvature for the specimens. The flattening out of loads at various times, as well as jumps in the force, are due to the load and unload points as the test was paused to inspect the beam for cracks.

**Table 3.** Initial and effective prestressing forces measured by embedded vibrating-wire strain gauges

| Specimen | $P_i$, kip | $P_e$, kip |
|---|---|---|
| PS-0R-NC | 90.4 | 86.9 |
| PS-SR-NC | 100.4 | 94.0 |
| PS-SR-C | 93.7 | 83.0 |

Note: $P_e$ = effective prestress force; $P_i$ = initial prestressing force.
1 kip = 4.448 kN.

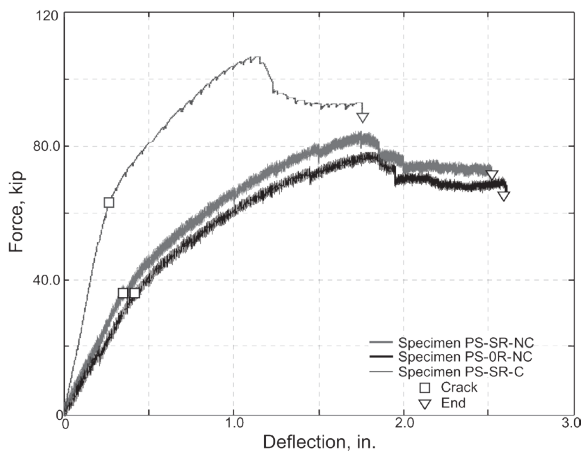


Load versus deflection

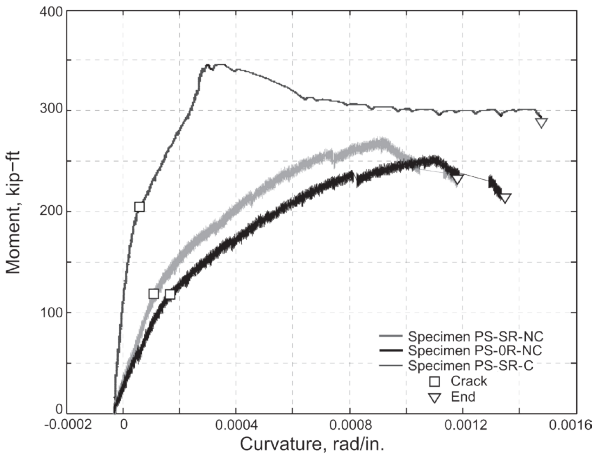


Moment versus curvature

**Figure 5.** Comparison of beam specimens. Note: 1 in. = 25.4 mm; 1 kip = 4.448 kN; 1 rad/in. = 0.039 rad/mm; 1 kip-ft = 1.356 kN-m.

## Specimen PS-SR-NC

Specimen PS-SR-NC contained the required amount of shear reinforcement according to the AASHTO LRFD specifications,[13] ignoring the contribution of the fibers to the shear capacity. The effective prestressing force at the time of testing was approximately 94.0 kip (418 kN).

The shear behavior of the specimens was monitored using strain gauges that were fixed to the inside face of shear stirrups close to the south support. The maximum measured strain corresponded to a stress of approximately 580 psi (4000 kPa) in the stirrup leg. No shear cracks were observed throughout the testing of the beam specimen.

The string potentiometers at the quarter spans recorded nearly identical displacements, indicating that the behavior of the specimen was symmetric. The deflection captured at the ultimate load of 84.7 kip (377 kN) by the midspan string potentiometers was approximately 1.75 in. (44.5 mm). The deflections of the quarter spans at the ultimate load were approximately 1.09 and 1.15 in. (27.7 and 29.2 mm) for the north and south quarter-span sensors, respectively.

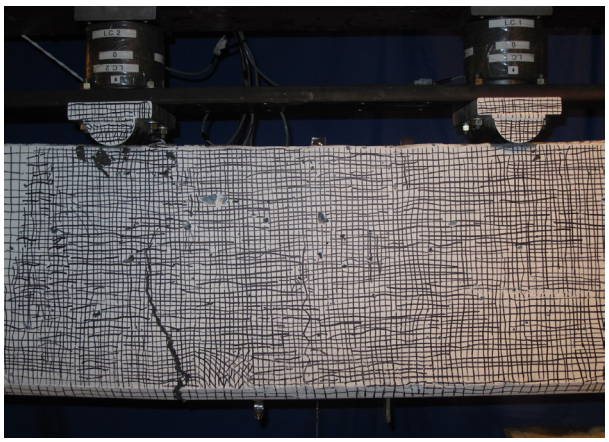

East face of specimen

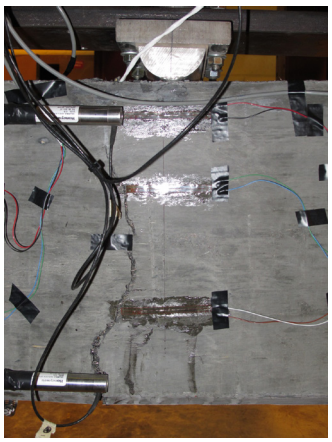

West face of specimen

**Figure 6.** Failure crack for specimen PS-SR-NC.

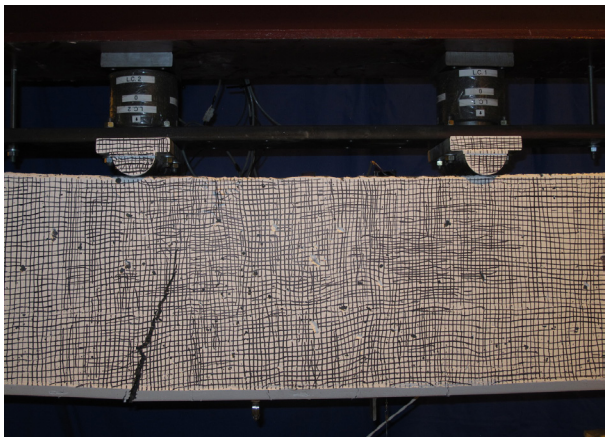

Failure crack on east face

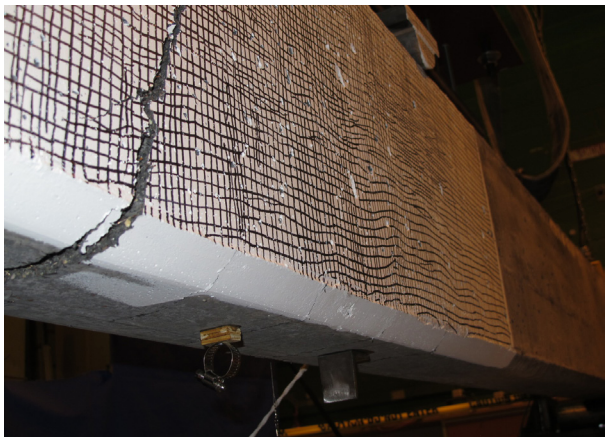

Failure crack and closely spaced adjacent flexural cracks on east face

**Figure 7.** Specimen PS-0R-NC.

Figure 5 shows the load-deflection behavior of the prestressed UHPC beam specimen. The specimen maintained its initial stiffness until it reached a deflection of approximately 0.35 in. (8.9 mm) at a force of 36.3 kip (162 kN). The load-deflection behavior then began to soften until the beam reached its ultimate load. The load then quickly dropped while the beam continued to undergo significant inelastic deformations. The test was stopped at a deflection of 2.50 in. (63.5 mm).

The moment-curvature behavior (Fig. 5), remained primarily elastic until the point of observed cracking, corresponding to a moment of 118 kip-ft (160 kN-m). The specimen continued to soften until the peak moment of 275 kip-ft (373 kN-m), after which the moment-carrying capacity quickly dropped until the test was stopped.

Failure occurred approximately 1.50 ft (0.457 m) south of center span as one crack began to propagate and widen. **Figure 6** provides images from both the east and west face of the specimen at the failure load. The failure crack occurred outside of the linear variable displacement transducer range and stopped approximately 3.75 in. (95.3 mm) from the top of the specimen. Significant fiber pullout had occurred by this point and the flexural behavior began to flatten out as the strands continued to yield.

## Specimen PS-0R-NC

Specimen PS-0R-NC contained no mild steel reinforcement, assuming that all shear forces would be carried by the concrete and steel fiber reinforcement. The effective prestressing force at the time of testing was approximately 86.9 kip (387 kN).

The string potentiometer data at the quarter spans were not as symmetric as in the testing of specimen PS-SR-NC; however, overall the behavior was relatively similar at each end. The midspan deflection captured at the ultimate load of 78.4 kip (349 kN) was approximately 1.71 in. (43.4 mm). The deflections of the quarter spans at ultimate load were approximately 1.11 and 1.20 in. (28.2 and 30.5 mm) for the north and south quarter-span sensors, respectively.

Figure 5 shows the deflection versus load behavior of the specimen. Similar to specimen PS-SR-NC, the specimen maintained its initial stiffness until it reached a deflection of approximately 0.42 in. (11 mm) at a force of 36.1 kip (161 kN), corresponding to the point of observed cracking. The behavior began to soften at this point until the beam reached its ultimate. After reaching its peak load, the load quickly dropped while the beam continued to undergo significant inelastic deformations. The test was stopped at a deflection of 2.60 in. (66.0 mm).

Figure 5 shows the curvature versus moment behavior of the specimen. The specimen behavior remained primarily elastic until the point of observed cracking, corresponding to a moment of 117.4 kip-ft (159.2 kN-m). The specimen continued to soften until the peak moment of 255 kip-ft (345 kN-m), after which the moment-carrying capacity quickly dropped until loading was stopped.

Despite the elimination of shear reinforcement, little difference was observed in the flexural behavior of specimen PS-0R-NC from the flexural behavior of specimen PS-SR-NC. The shear region of the beam underwent shear forces of approximately 40 kip (178 kN) with no visually observed shear cracking. This indicates that fiber-reinforced concrete had enough shear capacity to allow a flexure failure mode before premature failure in shear. The failure of the specimen resulted from the widening and propagation of a single crack located almost directly under the south load

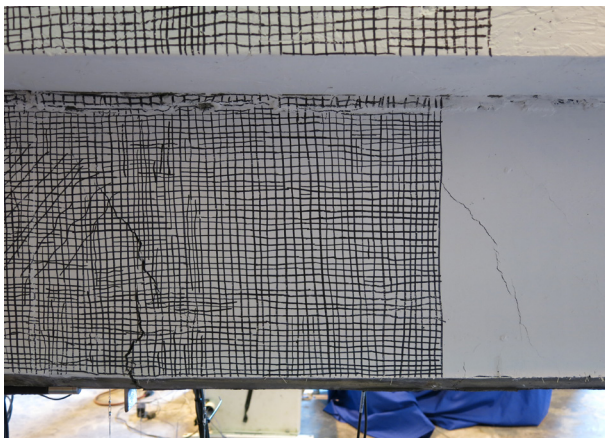

Flexural failure crack (left) and flexural-shear crack 2.0 ft (0.61 m) from center span (right) on east face

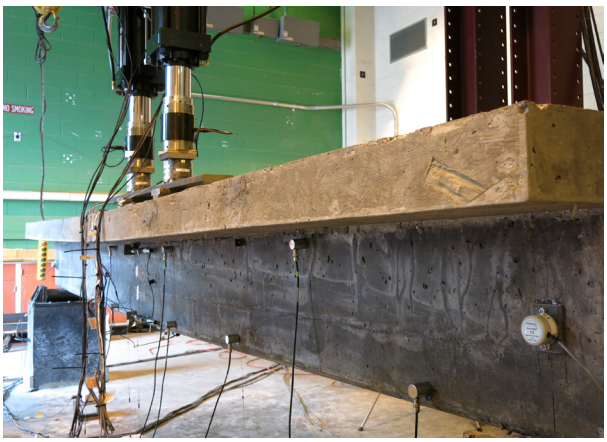

Span deflection at failure

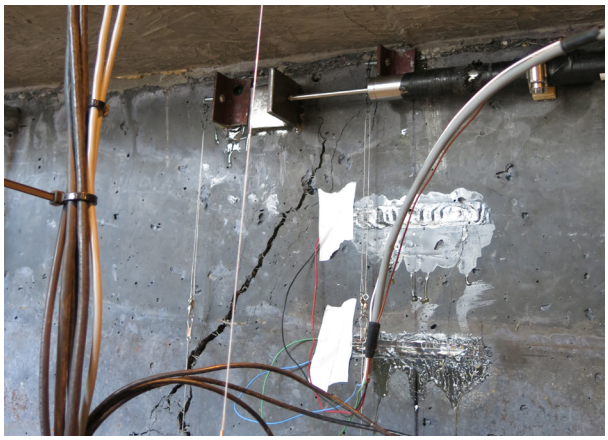

Crack propagation into composite slab at failure

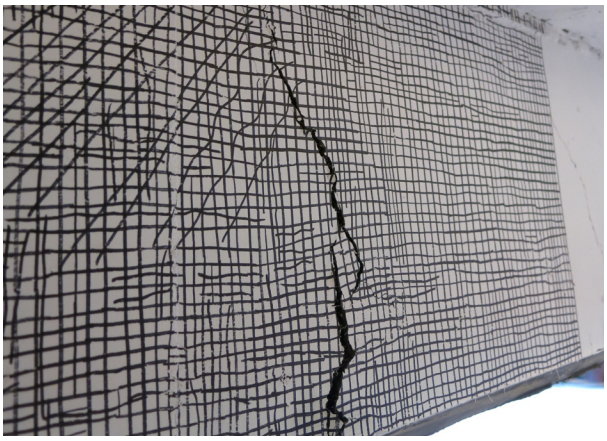

Flexure crack at midspan on east face

**Figure 8.** Cracked regions of specimen PS-SR-C.

point (**Fig. 7**). Significant fiber pullout occurred within the failure crack, which extended from the bottom face of the specimen up to approximately 4.0 in. (100 mm) from the top face.

## Specimen PS-SR-C

Specimen PS-SR-C was similar to specimen PS-SR-NC and possessed a composite cast-in-place HSC deck. The effective prestressing force at the time of testing was approximately 83.0 kip (369 kN).

Similar to PS-SR-NC, specimen PS-SR-C's shear behavior of was captured by placing strain gauges on the inside faces of shear stirrups close to the south support. The strains remained small throughout the test, and the largest recorded strain was 7.5 με. This is equivalent to a stress of 218 psi (1500 kPa) in one leg of the stirrup, indicating that the stirrups were minimally engaged.

The two string potentiometers located directly at center span recorded almost identical displacements throughout testing until the sensor fixed to the UHPC beam began to show a slight increase in its recorded deflection compared with the sensor on the HSC deck at ultimate loads. This was most likely due to the slight separation that occurred between the deck and beam as the composite reinforcement was engaged. The deflections of the string potentiometers at center span at ultimate loads were equal to 1.16 and 1.14 in. (29.5 and 29.0 mm) for the sensors attached to the UHPC beam and HSC deck, respectively. As observed in the previous two tests, the north quarter point experienced slightly smaller deflections than the south quarter point at the ultimate load, with magnitudes of 0.74 and 0.79 in. (19 and 20 mm), respectively.

Figure 5 shows the deflection versus load plot of the specimen. Similar to the other specimens, the composite beam maintained its initial stiffness until it reached a deflection of approximately 0.267 in. (6.78 mm) at a force of 63.1 kip

(281 kN), corresponding to the point of observed cracking. However, the stiffness of the beam was larger due to the larger composite cross-sectional area. The deflection versus load behavior began to soften once cracking occurred until the beam reached its ultimate load-carrying capacity. The load then quickly dropped while the beam continued to undergo significant inelastic deformations. The test was stopped at a deflection of 1.75 in. (63.5 mm).

Figure 5 shows the curvature versus moment behavior for specimen PS-SR-C. The specimen behavior remained primarily elastic until the point of observed cracking, corresponding to a moment of 205 kip-ft (278 kN-m). The specimen continued to soften until the peak moment of 346 kip-ft (469 kN-m). The moment-carrying capacity then quickly dropped while the curvature continued to increase without an increase in load-carrying capacity until loading was stopped.

The failure of specimen PS-SR-C resulted after a single crack eventually propagated through the entire UHPC beam and up to approximately 2.50 in. (63.5 mm) below the top surface of the deck. This crack quickly grew larger than the surrounding cracks and led to the failure of the specimen. The beam behaved fully composite because there was minimal separation observed between the deck and the UHPC beam.

Unlike the previous two specimens, specimen PS-SR-C developed flexural-shear cracks as it was loaded. These cracks became visible at a load of approximately 51.2 kip (228 kN) and continued to widen throughout the test. However, these cracks did not lead to beam failure, and eventually flexure cracks at the midspan of the specimen widened and led to the ultimate flexural failure of the specimen. The flexural-shear cracks occurred approximately 2.0 ft (0.61 m) north of the beam center span, with a calculated shear force in that region of 26.3 kip (117 kN). Once the flexural-shear cracks became clearly visible, fibers could be seen across them and likely prevented these cracks from continuing to propagate. Despite the flexural-shear cracking, shear cracking was not visually observed near the support and the maximum measured strain in the shear stirrups near the support remained low and corresponded to a stress of approximately 218 psi (1.50 MPa), indicating that shear cracking did not occur in the highest shear region near the support. **Figure 8** provides images taken during testing of the specimen, showing the flexural-shear crack north of center span, the flexural failure crack at midspan, and the crack propagation into the composite HSC deck.

## Discussion

### Global behavior

**Table 4** compares the experimental moment capacities of the three beam specimens with the AASHTO LRFD specifications[13] design moment capacity. The moment capacities were significantly above the design strengths. As the specimen was loaded, cracks on the bottom face of the specimen became apparent shortly after the measured point of cracking. Failure occurred due to the eventual widening of one of these cracks and was due to the combined effects of concrete crushing (in the UHPC in the two noncomposite beams and in the HPC in the composite beam), strand yielding (in all three beams, determined based on measured concrete strains at the level of the strands), and fiber pullout.

**Table 4.** Comparison of design moment capacity with maximum measured moment during flexural testing

| Source | Moment capacity, kip-ft | | |
|---|---|---|---|
| | PS-SR-NC | PS-0R-NC | PS-SR-C |
| 2012 AASHTO LRFD specifications section 5.7.3 | 174 | 174 | 254 |
| Maximum applied at peak flexural resistance | 275 | 255 | 346 |
| Ratio | 1.58 | 1.47 | 1.36 |

Note: 1 kip-ft = 1.356 kN-m.

## Elimination of shear reinforcement

Eliminating shear reinforcement from the specimens should have little impact on the flexural behavior of the specimen unless the shear capacity of the concrete is exceeded in the regions near the supports. The shear forces carried in these regions were approximately 41 and 39 kip (180 and 170 kN) for specimens PS-SR-NC and PS-0R-NC at ultimate flexural resistance, respectively. No visible sign of shear cracking was observed during the testing of either specimen, and the strain gauges that were instrumented to the first stirrups close to the south roller support recorded negligible strain during testing of specimens PS-SR-NC and PS-SR-C. **Table 5** provides the applied loads developed during flexural testing, ultimate cal-

**Table 5.** Comparison of design shear capacities with maximum measured shear forces during flexural testing

| Source | Shear capacity, kip | | |
|---|---|---|---|
| | PS-SR-NC | PS-0R-NC | PS-SR-C |
| 2012 AASHTO LRFD specifications section 5.8.3.3 | 58.5 | 23.3 | 79.1 |
| Maximum applied at peak flexural resistance | 43.6 | 39.8 | 51.8 |
| 2002 AFGC/SETRA *Ultra High Performance Fiber-Reinforced Concrete* | 200 | 165 | 221 |

Note: 1 kip = 4.448 kN.

culated capacities of the specimens according to the AASHTO LRFD specifications,[13] and the capacities of the specimens incorporating fiber shear strength, following Ulm[22] and Association Française de Génie Civil/Service d'Études Techniques des Routes et Autoroutes (AFCG/SETRA).[15]

Following the AASHTO LRFD specifications,[13] the fiber contribution to shear capacity is ignored. The AFGC-SETRA[15] recommendations for the shear capacity of fiber reinforcement were used to calculate the shear capacities (Table 5). Due to the rectangular cross section, the shear contribution of the fibers was significant and increased the calculated shear capacities by approximately 142 kip (631 kN).

Excluding fiber contribution on the ultimate shear strength, specimen PS-0R-NC was loaded significantly past the predicted shear capacity according to the AASHTO LRFD specifications.[13] The load applied was approximately 71% larger than the AASHTO-predicted capacity, which is based on the concrete strength contribution to shear (ignoring fiber contributions). This indicates that the fibers significantly increased the total shear capacity of the specimen. Also, strains from the shear stirrups in specimen PS-SR-NC measured close to zero strain in the shear stirrups closest to the south support, providing evidence that shear cracking did not occur and engage the reinforcement. No inclined cracks were observed in the shear regions, aside from flexure-shear cracks observed during the testing of specimen PS-SR-C. However, these cracks did not lead to the failure of the specimen, and propagation was halted shortly after formation. Eventually this specimen failed due to flexure within the moment region of the beam, with a vertical crack propagating through the entire UHPC member and halfway into the composite HSC deck. Figure 5 provides a direct comparison of the flexural behavior of specimens with and without shear reinforcement. According to the AASHTO LRFD specifications, the shear capacity of specimen PS-0R-NC should have been reached shortly after the measured cracking point; however, it is clear that the specimen continued to carry significant shear forces until flexural failure.

There was no observable difference in the behavior of the specimens under flexural testing. The shear spans of the specimens were visually observed throughout testing to locate the formation of any shear cracking. However, no observable shear cracks were found, aside from a flexure-shear crack that formed in the web of specimen PS-SR-C approximately 1.0 ft (305 mm) from the north load point. This provides preliminary evidence that correlates with results from testing on other proprietary UHPCs, suggesting that removal or reduction of shear reinforcement is possible due to the additional shear capacity provided by the fibers. The test setup was not designed to assess shear capacity, and the values presented are the shear forces developed during flexural testing.

## Effect of composite deck

The addition of composite, cast-in-place concrete decks is common practice in prestressed bridge superstructure construction. Therefore, there was an interest in how the fiber-reinforced UHPC would contribute to the strength of a beam with a much lower-strength concrete in the primary compression region. There was concern that the deck concrete would reach its ultimate compressive stress and crush before the full contribution of fibers in the UHPC section.

The concrete deck behaved fully composite, and little to no difference was observed between deflections in the deck and adjacent deflections in the composite UHPC beam at center span. The composite section had a much stiffer measured behavior and was able to carry significant loads before cracking. Full fiber engagement (that is, the entire cross section is cracked and in tension) was predicted to occur shortly before steel yielding, meaning that midspan flexural cracks should have visually spread into the deck concrete before ultimate loads were reached. This correlated well with observations, which showed the crack propagating into the deck. Failure was likely due to a combination of strand yielding, concrete crushing, and fiber pullout at the extreme tension regions of the girder.

The concrete deck significantly increased capacities by creating a much stiffer section with a large region to resist compressive forces and also allowed for the full engagement of fibers within the UHPC cross section. Because the neutral axis was within the deck at ultimate loads, the entire UHPC beam was able to contribute to the tensile strength of the section.

Although the placement of a cast-in-place HSC deck in composite action with a UHPC girder provided clear benefits to the flexural strength, the long-term effectiveness of the specimen will still need to be investigated. Because of the shorter expected lifespan of HSC compared with UHPC, it is possible that the deck concrete would need to be replaced before the UHPC reaches its full design life. Furthermore, if using a HSC deck, designers who desire to take advantage of the tensile capacity of the UHPC fibers will need to ensure that the composite beam is proportioned to ensure that the neutral axis remains in the deck at ultimate.

## Conclusion

Three UHPC beams—one with typical steel reinforcement, one with minimal steel reinforcement, and one with typical steel reinforcement and a composite slab—were designed, constructed, and monitored during testing to failure. The flexural capacities for all beams exceeded design estimations, thus demonstrating the feasibility of incorporating UHPC into transportation infrastructure projects. The moment capacity was significantly higher than the predicted values (ratios of 1.58, 1.47, and 1.36 for the three beams) due to the improved mechanical properties and the contributions of the steel fibers.

The shear demand for each of the specimens exceeded the strength predicted by design, and each carried the developed shear forces, even in the specimen without mild steel shear reinforcement. No shear cracks were observed in the two beams without the composite slab. Mild flexural-shear cracking in

the composite beam was observed, but these cracks remained tightly closed. This demonstrated the significant contribution of the steel fibers to the shear capacity.

Fully composite action was developed between the UHPC beam and HSC deck. Negligible slip was observed throughout the loading history. As the loading increased, the neutral axis was able to migrate into the deck.

## Acknowledgments

This research was partially funded by the PCI Daniel P. Jenny Fellowship and the New Mexico Department of Transportation (Keli Daniell, project manager). The batching, casting, and curing of the large-scale specimens investigated in this project could not have been accomplished without the team at Coreslab Structures (ALBUQUERQUE) Inc. Material donations and assistance were provided by Jobe Materials LP, Mona Gomez with El Paso Machine and Steel, Todd Fraker with Dayton Superior, David C. Parham with Bekaert Corp., Darren Jewell with BASF, and Doug Martin with Voss Engineering. Assistance in the laboratory and field was provided by graduate student Mark Manning and undergraduate research assistants Rafael Garcia and Janice Gossett. The materials and assistance provided are greatly appreciated.

## References

1. Graybeal, B. 2008. "UHPC in the U.S. Highway Transportation System." In *Ultra-High Performance Concrete (UHPC): Proceedings of the Second International Symposium on Ultra High Performance Concrete, Kassel, Germany, March 5–7, 2008*. Kassel, Germany: Kassel University Press.

2. Weldon, B. D., D. V. Jauregui, C. M. Newtson, C. W. Taylor, K. F. Montoya, and S. Allena. 2010. *Feasibility Analysis of Ultra High Performance Concrete for Prestressed Concrete Bridge Applications*. Report NM09MSC-01. Albuquerque, NM: New Mexico Department of Transportation.

3. Taylor, C. W., B. D. Weldon, D. V. Jauregui, and C. M. Newtson. 2013. "Case Studies Using Ultra High-Performance Concrete for Prestressed Bridge Design." *Practice Periodical on Structural Design and Construction* 18 (4): 261–267.

4. Weldon, B., D. Jauregui, C. Newtson, K. Montoya, C. Taylor, S. Allena, J. Muro, M. Tahat, E. Lyell, and E. T. Visage. 2012. *Feasibility Analysis of Ultra High Performance Concrete for Prestressed Concrete Bridge Applications–Phase II*. Report NM09MSC-01. Albuquerque, NM: New Mexico Department of Transportation.

5. Lyell, E. K., J. Muro, C. M. Newtson, B. D. Weldon, D. V. Jauregui, and S. Allena. 2012. "Optimization of Ultra High Performance Concrete Mixture Proportions Using Locally Available Materials." In Twelfth International Conference on Recent Advances in Concrete Technology and Sustainability Issues, Prague, Czech Republic, October 31–November 2, 2012. Detroit, MI: ACI.

6. Muro-Villanueva, J., C. Newtson, S. Allena, B. Weldon, and D. Jauregui. 2012. "Freezing and Thawing Durability of Ultra-high Strength Concrete." In *International Congress on Durability of Concrete Proceedings, Trondheim, Norway, June 18–21, 2012*. Oslo, Norway: Norwegian Concrete Association.

7. Ahlborn, T. M., D. Li Misson, E. J. Peuse, and C. G. Gilbertson. 2008. "Durability and Strength Characterization of Ultra-high Performance Concrete under Variable Curing Regimes." In *Ultra High Performance Concrete (UHPC): Proceedings of the Second International Symposium on Ultra High Performance Concrete, Kassel, Germany, March 5–7, 2008*. Kassel, Germany: Kassel University Press.

8. Graybeal, B. A. 2006. *Material Property Characterization of Ultra High Performance Concrete*. FHWA-HRT-06-103. Washington, DC: Federal Highway Administration.

9. Giesler, A. J., S. B. Applegate, and B. D. Weldon. 2016. "Implementing Nonproprietary Ultra-high-performance Concrete in a Precasting Plant." *PCI Journal* 61 (6): 68–80.

10. Guaderrama, L. R., and B. D. Weldon. 2013. "Compressive Stress-Strain Behavior of Ultra High Performance Concrete Using Local Materials." Paper presented at the TRB 92nd Annual Meeting, Washington, DC, January 13–17, 2013.

11. ASTM Subcommittee C09.61. *Standard Test Method for Flexural Strength of Concrete (Using Simple Beam with Third-Point Loading)*. ASTM C78-09. West Conshohocken, PA: ASTM International.

12. Visage, E. T. 2013. "Experimental Analysis of the Flexural Behavior of Ultra-High Performance Concrete Beams Using Local Materials." MS thesis, New Mexico State University, Las Cruces, NM.

13. AASHTO (American Association of State and Highway Transportation Officials). 2012. *AASHTO LRFD Bridge Design Specifications*. 6th ed., customary U.S. units. Washington, DC: AASHTO.

14. Naaman, A. E., and H. W. Reinhardt. 2006. "Proposed Classification of HRFRC Composites Based on Their Tensile Response." *Materials and Structures* 39 (5): 547–555.

15. AFGC/SETRA (Association Française de Génie Civil/Service d'Études Techniques des Routes et Autoroutes). 2002. *Ultra High Performance Fiber-Reinforced Concrete – Interim Recommendations*. Paris, France: AFGC/SETRA.

16. JSCE (Japan Society of Civil Engineers) Subcommittee on Research of Ultra High Strength Fiber Reinforced Concrete. 2006. *Recommendations for Design and Construction of Ultra High Strength Fiber Reinforced Concrete Structures*. Tokyo, Japan: JSCE.

17. Gowripalan, N., and R. I. Gilbert. 2000. "Design Guidelines for Ductal Prestressed Concrete Beams." Reference article prepared for VSL Australia. Sydney, Australia: School of Civil and Environmental Engineering, The University of New South Wales.

18. Graybeal, B. A. 2007. "Compressive Behavior of Ultra-high-performance Fiber-Reinforced Concrete." *ACI Materials Journal* 104 (2): 146–152.

19. ASTM Subcommittee C09.61. 2014. *Standard Test Method for Compressive Strength of Cylindrical Concrete Specimens*. ASTM C39/C39M-14a. West Conshohocken, PA: ASTM International.

20. BSI (British Standards Institution). 1983. *Testing Concrete. Method for Determination of Compressive Strength of Concrete Cubes*. BS 1881-116. London, UK: BSI.

21. Giesler, A. J. 2014. "The Flexural Behavior and Analysis of Prestressed Ultra High Performance Concrete Beams Made from Locally Available Material." MS thesis, New Mexico State University, Las Cruces, NM.

22. Ulm, F. J. 2004. "Bending and Shear Design of Iowa DOT Sample Bridge—Update." Department of Civil and Environmental Engineering, Massachusetts Institute of Technology, Cambridge, MA.

## Notation

$A_f$ = area of the cross section in tension between the neutral axis and centroid of prestressing steel

$A_{ps}$ = prestressing strand area

$A_s$ = longitudinal mild steel reinforcement area

$E_c$ = concrete modulus of elasticity

$f'_c$ = specified compressive strength of concrete

$f_{c,7day}$ = concrete compressive strength at seven days

$f_{c,28day}$ = concrete compressive strength at 28 days

$f_{c,test}$ = test day compressive strength

$f_{f,U}$ = tensile strength of crack-bridging fibers

$f_{ps}$ = stress at the centroid of prestressing strands at ultimate loads

$f_{pu}$ = ultimate strand tensile strength

$f_{py}$ = yield strength

$f_r$ = modulus of rupture

$f_s$ = stress in the mild steel reinforcement

$M_n$ = nominal moment strength

$P_e$ = effective prestressing force

$P_i$ = initial prestressing force

$v_f$ = fiber content as percentage of volume

$V_c$ = shear strength of concrete

$V_f$ = shear strength of steel fibers

$V_n$ = nominal shear strength

$V_P$ = shear strength of prestressing strand

$V_s$ = shear strength of the mild steel shear reinforcement

*w/cm* = water–cementitious material ratio

$z_f$ = distance between the resultant of the fiber tensile strength and the concrete compression resultant

$z_{ps}$ = distance between the resultants of tension in prestressing strands and compression in the concrete

$z_s$ = distance between the resultants of force in the mild steel and compression in the concrete

$\beta_f$ = fiber stress distribution factor

$\varepsilon$ = strain

$\varepsilon_{f,lim}$ = ultimate tensile strain

$\sigma$ = stress

$\phi$ = strength-reduction factor

$\phi_c$ = strength-reduction factor for concrete

$\phi_f$ = strength-reduction factor of steel fibers to account for the variability of fiber dispersion

$\phi_s$ = LRFD mild steel strength-reduction factor for shear = 0.9

$\phi_v$ = strength-reduction factor for shear

## About the authors


Andrew J. Giesler, PE, is a structural engineer with Dekker/Perich/Sabatini in Albuquerque, N.Mex. Giesler has performed the structural engineering for an array of building types constructed throughout New Mexico, as well as other parts of the western United States, including Southern California, Colorado, and Idaho.

Michael J. McGinnis, PhD, PE, is an associate professor in the department of civil engineering at the University of Texas at Tyler. His research interests include studying ultra-high-performance concrete use in bridge girders to reduce weight and increase design life using the core drilling method to determine in-place stress in concrete and in-place prestressing force in bridge girders and using digital image correlation to monitor structural testing of infrastructure systems and evaluating the suitability of recycled concrete aggregates for structural concrete applications. He earned his PhD from Lehigh University in Bethlehem, Pa., in 2006.

Brad D. Weldon, PhD, is an associate professor in the department of civil engineering at New Mexico State University in Las Cruces, N.Mex.


## Abstract


Ultra-high-performance concrete (UHPC) is a cementitious material with a dense microstructure. This contributes to high compressive strengths, as well as enhanced durability properties resulting in improved, sustainable construction. The material also possesses significant postcracking strength and ductility due to the addition of steel fibers. These characteristics produce a material that provides advantages over conventional concrete; however, the high costs of materials and production, lack of industry familiarity, and absence of standardized design procedures have impeded its widespread use.

Producing UHPC with locally available materials creates a more economical product. This research focused on the design, flexural testing, and analysis of three large-scale prestressed beams using UHPC mixture proportions developed with materials local to the state of New Mexico. Parameters varied among the prestressed specimens and included the removal of all mild steel reinforcement and the effect of a composite cast-in-place concrete deck. Experimental strengths were compared to design strengths according to the American Association of State Highway and Transportation Officials' *AASHTO LRFD Bridge Design Specifications*.


## Keywords


Experimental testing, local materials, UHPC, ultra-high-performance concrete.